Water Practice & Technology

IWA PUBLISHING

Performance evaluation of a nonstandard Parshall flume and comparison of experimental techniques for its verification in a drinking water treatment plant

José Gabriel León [a,*], José Manuel Díaz Lozada[a,b], Ana Inés Heredia Ligorria[c], Adriana Beatriz Muchiut[d], Gabriel Sentlinger[e], Carlos Gastón Catalini[f], Carlos Marcelo García[g] and Iván Matías Ragessi[h]

[a] National Water Institute and National Scientific and Technical Research Council, Medrano 235, Villa Carlos Paz, Argentina
[b] Faculty of Exact, Physical and Natural Sciences, National University of Cordoba, Medrano 235, Villa Carlos Paz, Argentina
[c] National Water Institute and Faculty of Exact, Physical and Natural Sciences, Av. Vélez Sarsfield 1611, Córdoba, Argentina
[d] Villa Carlos Paz City Government, Liniers 50, Villa Carlos Paz, Argentina
[e] Fathom Scientific Ltd, 1561 Whitesails Dr, Bowen Island, BC V0N1G2, Canada
[f] Faculty of Engineering, Catholic University of Cordoba and National Water Institute, Medrano 235, Villa Carlos Paz, Argentina
[g] Institute for Advanced Studies for Engineering and Technology (CONICET/UNC) – Faculty of Exact, Physical and Natural Sciences, National University of Cordoba, Av. Vélez Sarsfield 1611, Córdoba, Argentina
[h] Faculty of Engineering, Catholic University of Cordoba and Faculty of Exact, Physical and Natural Sciences, National University of Cordoba, Bv. Dr Juan Filloy s/n, Córdoba, Argentina
*Corresponding author. E-mail: jleon@ina.gob.ar

(iD) JGL, 0000-0001-7051-7863

ABSTRACT

This article investigates a nonstandard Parshall flume (Pf) to assess the impact of engineering deficiencies on flow rate (Q) estimation and compare experimental techniques for evaluating its performance in Q quantification and velocity gradient (G) appraisal during rapid mixing. Considering construction and instrumentation issues in the studied Pf, Q estimates were 10% lower than those derived from the standard rating curve (SRC), with 9% of this discrepancy attributable to the high placement of the stilling well scale and 1% to the position of the connecting pipe to the gauging section. When contrasting Q estimates from the SRC to the current rating curve in use and a set of rating curves fitted using salt dilution gauging (SDG), acoustic Doppler velocimetry (ADV), and numerical modeling (CFD), the average differences were -10.2, -8.3, -2.2, and 0.2%, respectively, for the current rating curve in use and those fitted to ADV, SDG, and CFD data. Considering only the instrumental measuring techniques, the SDG exhibited superior fittings ($R^2 = 0.99$), followed by ADV ($R^2 = 0.95$). Calculations of G aligned (9.3%) with CFD estimates support these methods as reliable tools for evaluating and verifying nonstandard Pf performance.

Key words: acoustic Doppler velocimetry, computational fluid dynamics, mixing, Parshall flume, salt dilution gauging, water treatment

HIGHLIGHTS

- Novel methodologies are used to evaluate the fitting of Parshall flume (Pf) standard rating curves (SRCs) in nonstandard Pf installations.
- Comparative accuracy of Q estimation techniques is addressed demonstrating the superior accuracy of salt dilution gauging in fitting rating curves compared with the SRC.
- Verification of performance evaluation through computational fluid dynamics is supported by closely matching the SRC.

GRAPHICAL ABSTRACT
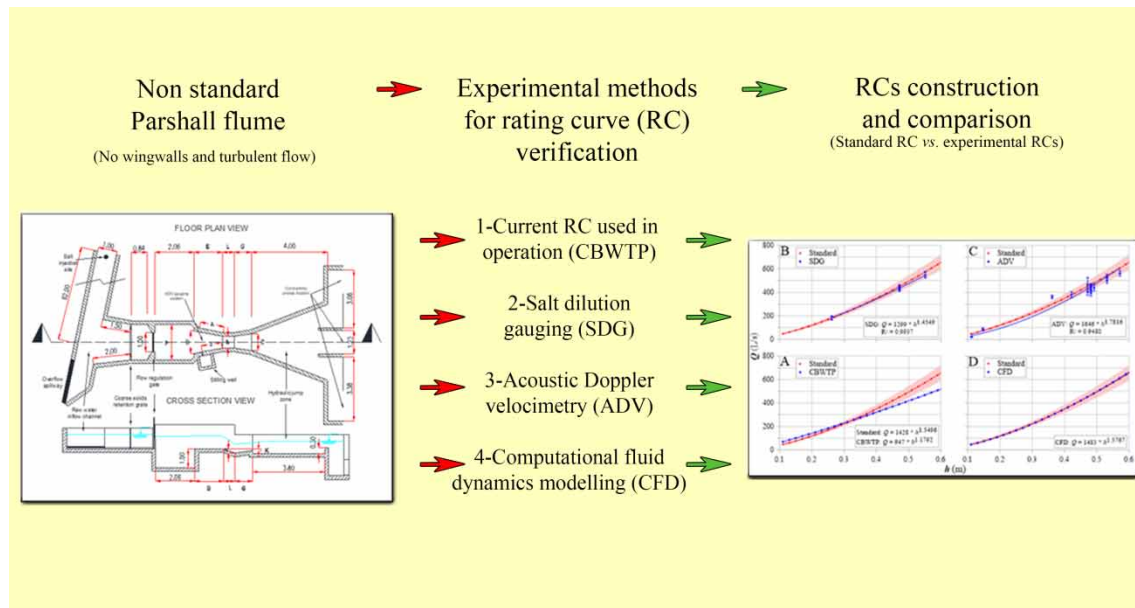
1. INTRODUCTION

In a water treatment process, it is essential to carry out reliable estimates of the flow rate (Q) of raw water entering the plant. This variable, in addition to assessing the water quantity extracted from a source, controls basic operating parameters such as the concentration of dosed chemicals and the residence time and intensity of agitation in hydraulic devices (McCabe *et al.* 2005). In this sense, for a specific design, the efficiency of these operations depends on Q; therefore, its accurate and continuous estimation is a fundamental condition to optimize the overall performance of the system.

The Parshall flume (Pf) is a widely used device for measuring Q in water treatment systems. Its operation is based on measuring the hydraulic head (h) generated by a constriction in a channel, which is directly proportional to the volumetric flow rate upstream of this constriction (Hendricks 2011). This section is referred to as the primary system and must have specific proportions among its dimensions. The primary system is complemented by a water level measuring instrument, known as the secondary system, which records the value of h (Davis 2019). The h value is converted into a Q value using a size-specific rating curve (RC) developed by R.J. Parshall and tested and improved over the years (Heiner *et al.* 2011). Apart from being relatively simple to construct, operate, and maintain, these devices offer advantages such as low head loss, a broad range of operating Q, and the potential to serve as a hydraulic rapid mixing device. However, there are studies documenting inaccuracies in Q estimation derived from installations that do not respect standardized lengths and/or fail to consider the characteristics of the approach flow (ref. in Khosronejad *et al.* (2021)). Therefore, to obtain adequate performance, it is necessary for the device to carefully adhere to the established dimensions and undergo periodic checks and verifications, ensuring that the obtained pairs of h, and Q values fit with the standard RC (SRC) (USEPA 2017). If the construction dimensions do not match those of a standard device, the system can be calibrated by applying reliable Q estimation techniques (Silva Ribeiro *et al.* 2021). This involves building a scatterplot of h, Q pairs and calculating the degree of divergence between the values obtained experimentally and those estimated from the SRC (Wright *et al.* 1994; ASTM 2001; Khosronejad *et al.* 2021; Vatankhah 2022).

As indicated above, the mixing processes in the reactors that make up a water treatment system depend on Q. In this sense, due to its impact on downstream operations, the rapid mixing process is of particular importance. This process involves the instantaneous dispersion of chemicals in treatment water to destabilize colloidal particles, enabling their aggregation and subsequent separation by density difference (Bratby 2016). The evaluation of the efficiency of this process is generally conducted considering the mixing time (T) and the velocity gradient (G). These parameters account for both the duration and the intensity of agitation calculated from the

dimensions of the device and the volumetric flow through it. For this reason, once the RC in a nonstandard Pf is calibrated, it is necessary to verify that the values of T and G are within the optimal range considered.

In this article, a Pf that does not fully comply with construction recommendations was investigated: A series of Q estimations were conducted using three experimental techniques: (i) salt dilution gauging – SDG (Moore 2005); (ii) acoustic Doppler velocimetry – ADV (USGS 2004); and (iii) computational fluid dynamics – CFD (Heyrani *et al.* 2022). Our analysis focused on: (i) evaluating the performance of different Q estimation techniques under similar flow regime conditions, (ii) assessing the impact of using an SRC on Q readings in a nonstandard device, and (iii) using calculation and numerical modeling methods to determine the degree of similarity in estimates of rapid mixing parameters at the Pf hydraulic jump. The results were analyzed to assess the utility of these techniques to verify the RC and determine agitation intensity in rapid mixing.

2. METHODS

2.1. Study site

In this work, the performance of a Pf measuring the raw water inflow to the Cuesta Blanca Water Treatment Plant (CBWTP), located at 31°28′49.66″S, 64°35′6.81″W, was investigated. This plant supplies drinking water to the urban area of Villa Carlos Paz city and towns of the southern Punilla Valley, Córdoba, Argentina. The service supplies water to approximately 100,000 permanent residents, a number that triples during the summer season due to the fact the city is a tourist place. The treatment type is conventional and includes the following unit operations: (i) hydraulic rapid mixing in a Pf, (ii) flocculation with vertical shaft mechanical agitation and a 30° inclined blades impeller, (iii) lamellar sedimentation with hexagonal modules, (iv) downward flow rapid filtration with variable head loss and filtration rate, and (v) inline disinfection.

2.1.1. Description of the Parshall flume

The primary and secondary systems, along with their joint operation, were analyzed (ASTM 2001; ENOHSa 2001; USEPA 2017). This assessment covered the following aspects: (i) characteristics of the flow upstream of the device; (ii) dimensions and condition of materials (primary device); (iii) free discharge flow; and (iv) verification of the h measurement device (secondary device). According to information provided by CBWTP personnel, the current RC differs from the SRC for a 0.61 m throat Pf and there was no available information on how it was fitted.

2.1.1.1. Characteristics of the flow upstream of the device. Nonuniform flow upstream of the device was identified prior to the convergent section of the Pf. Four hydraulic singularities were observed generating turbulent flow movement (Figure 1): (i) Located immediately upstream of the beginning of the converging section lies a depression in the channel bed, measuring 1 m in depth and 2 m in length; this depression serves as the site for the intake of the secondary raw water supply system, facilitated through a DN600 pipe; (ii) a constriction in the channel where a flow regulation gate is mounted; (iii) a metal grid for filtering coarse material; and (iv) a curve at approximately 80° in the raw water transport channel, located within 5 m of the start of the convergent section.

2.1.1.2. Parshall flume dimensions and structure. In the original project of the CBWTP, a 0.61 m throat width Pf was adopted, suitable for operating Q between 12 and 900 L/s under free discharge conditions (ISO 1992; ASTM 2001). The primary system, constructed in 1987 with brick masonry and a fine concrete plaster, shows signs of wear and increased roughness. The differences between the dimensions of the CBWTP-Pf and the standard Pf fell mostly within $\pm 2\%$, as indicated by the ASTM (2001) standard. The most significant difference was observed in the height of the step at the end of the divergent section (K reference in Table 1), which is 23% higher than indicated in the standard design. Similarly, another difference with a standard device was the transition from the inlet channel to the converging section, where there were no wing walls. The walls connecting the channel with the converging section are perpendicular to the flow, generating turbulence. Additionally, the studied Pf lacks a 25% slope approach ramp prior to the beginning of the converging section (ASTM 2001). These differences from the standard design can be addressed for Q estimation by considering the correction coefficient developed by Heiner *et al.* (2011). Although computationally complex methodologies have been developed recently (e.g. Saran & Tiwari 2022), the coefficient proposed by Heiner *et al.* (2011) was preferred because it was developed using a physical model of a 0.61-m throat width Pf and
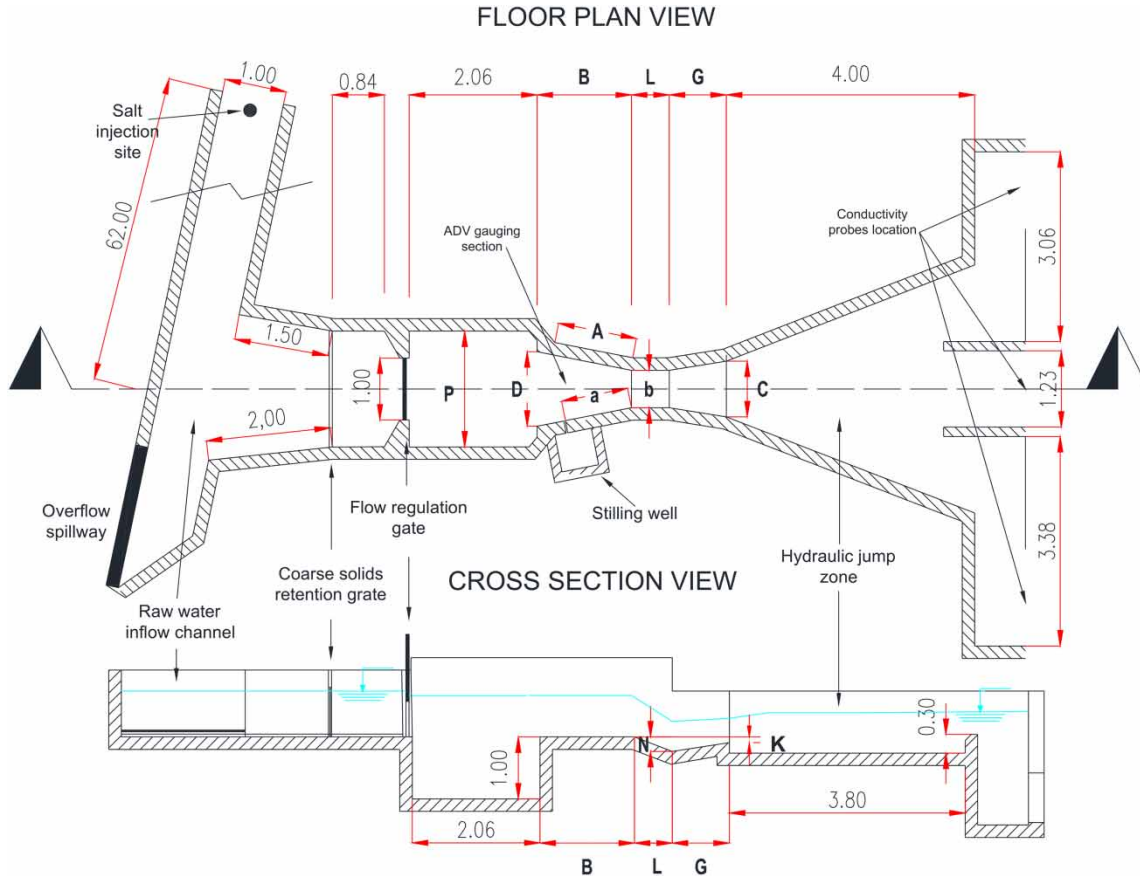
Figure 1 | As-built plan of the studied Pf. Distances referenced by letters are detailed in Table 1. The salt injection site for the SDG method is also shown.

Table 1 | Comparison between the dimensions of a standard Pf and those of the CBWTP

	b	A	a	B	C	D	L	G	K	P
Standard Pf (mm)	610	1,524	1,016	1,495	914	1,206	610	914	76	1,854
CBWTP-Pf (mm)	608	1,550	1,005	1,520	900	1,200	608	920	93	1,870
Difference (%)	−0.3	1.7	−1.1	1.7	−1.5	−0.5	0.3	0.7	23.0	0.9

considered the configuration without wing walls, which is the case studied in this article. These authors developed a set of equations to establish a correction coefficient applied to the Q estimated from the SRC and found that if the stilling well is located ~6 cm upstream of the flume's crest, the estimated Q from the Pf can be as much as 60% lower than the actual Q. The calculation of this coefficient in the studied Pf was performed using the equation defined by these authors for devices without guide walls or an approach ramp, referring specifically to the studied Pf:

$$C_{sw} = 1.691 \propto^5 - 7.052 \propto^4 + 11.01 \propto^3 - 8.444 \propto^2 + 3.571 \propto + 0.212 \tag{1}$$

where C_{sw} is the correction coefficient, and α is the location quotient of the inlet duct to the settling well relative to the design location (2/3 of the length of the wall of the convergent section). The C_{sw} coefficient is applied using the following formula:

$$Q_{corr} = \frac{Q_d}{C_{sw}} \tag{2}$$

where Q_{corr} is the corrected value of Q, and Q_d is the value of Q obtained from the SRC. The calculated value of C_{sw} was 0.9883, meaning that Q_{corr} is approximately 1% higher than the Q_d.

2.1.1.3. Free discharge flow.   Free flow in the discharge was verified by the ratio between depth in the measuring section (h_a) and depth before the hydraulic jump (h_b). In the studied Pf, this ratio was <0.50 for flow rates within the operating range. For a flume of these dimensions, free flow in the discharge exists when $h_a/h_b < 0.66$ (Hendricks 2011). Therefore, there is no need to use the Q correction technique considering the depths in the throat and in the divergent section.

2.1.1.4. Verification of the head measurement device.   The Pf secondary system comprises a stilling well equipped with a limnimetric scale and an associated ultrasonic level sensor. This structure, which has a square horizontal section measuring 0.60×0.60 m and a 1.3 cm diameter tube connecting it to the gauging section, has been found to be adequate for its intended purpose (ASTM 2001; Heiner *et al.* 2011; Savage *et al.* 2014). As this device records the values of h, from which Q is estimated using the corresponding RC, it is crucial to ensure that the zero level of the scale aligns with the bottom of the measuring section. Using an optical level (TI Asahi Co., Ltd, Saitama), it was determined that the zero point of the scale was 0.052 m above the level of the bottom of the measuring section. Consequently, the measurement obtained from this scale would be underestimating the Q by approximately 76 L/s, constituting about 13% of the maximum treatment Q (600 L/s).

2.2. Verification of the RC for the Parshall flume in Cuesta Blanca water treatment plant

2.2.1. Flow rate estimation by SDG

The slug injection method for SDG (Moore 2005) was used, which relies on the principle of continuity and assumes the complete incorporation and mixing of a tracer solution into a water stream to estimate its Q through mass balance equations (Boiten 2003). A sodium chloride (NaCl) solution was used (100 g NaCl in 2 L of channel water) to track concentration change from electrical conductivity (EC) measures in the Pf; i.e. concentration was estimated from EC using an experimentally determined coefficient relating both variables (Richardson *et al.* 2017). Flow rate estimations were performed using a QiQuac instrument (Fathom Scientific Ltd), which is a serial datalogging/conductivity apparatus intended to estimate Q in active watercourses with lateral mixing. A device equipped with three EC measurement probes with a resolution of 0.001 µS/cm and stability of 0.01% was used. This instrument computes the uncertainty of the Q estimate independently for each measurement probe, as well as the difference between the Q estimates from each probe (Sentlinger *et al.* 2019). Since the method is based on measuring the total mass of the tracer passing through the section, the use of three sensors can determine the independent quality of each estimation and any uncertainty due to incomplete mixing or other issues, such as the presence of a nonuniform velocity profile in the section. The EC measurement probes were placed 4 m downstream of the hydraulic jump, one in each channel that conveys coagulated water to each of the three treatment lines. This setup should ensure the complete mixing of the tracer solution required for this Q estimation method. However, if the hydraulic jump as a mixing feature is not taken into account, the calculated minimum mixing distance of the solution with the channel water (Pant *et al.* 2016) should be between 9.1 and 10.7 m. Considering these dimensions and to ensure the complete mixing, the NaCl solution was injected at the midpoint of the raw water inlet channel at a location ca. 75 m upstream the Pf (Figure 1). Eleven estimations were performed over a 4-h period during which no coagulant solution was dosed. The EC of the water at the beginning of the experiment was approximately 100 µS/cm, and producing peaks between 120 and 180 µS/cm after the tracer addition (Figure 3).

2.2.2. Flow rate estimation by ADV

An ADV FlowTracker2 instrument (SonTek, Xylem Inc.) was employed to estimate Q using the velocity–area method based on point velocity measurements in the convergent section of the cP (Figure 1) following the recommendations indicated by USGS (2004). The ADV, as the hydroacoustic instrument, is calibrated by the manufacturer and does not require subsequent calibration (Water Survey of Canada 2015). Estimations were performed using the mid-section method (ISO 2007), which involves dividing the gauging section into a number of stations formed by polygons of specific areas created for each station across the section. The velocity in each polygon is assumed to be equal to the average velocity calculated from a point velocity measurement. The gauging section in the studied device is 1.03 m wide and measurements were taken every 0.10 m, defining 11 verticals.

For each measured vertical, it was ensured that the control volume where the flow velocity is recorded was free of air bubbles, as these can affect proper instrument measurement. To obtain a representative value of the average velocity in the vertical, the sensor was placed at a height equivalent to 60% of the depth in the section when it was ≤0.50 m. For values >0.50 m, the sensor was positioned at two points: 20 and 80% of this height. Knowing the average velocity of each vertical, along with its width and depth, allows determining the Q of each vertical. The sum of these Q values provided the total Q of the section.

2.2.3. Flow rate estimation by CFD

This method provides a detailed insight into the flow patterns, allowing for a comprehensive estimation of Q (Heyrani *et al.* 2021, 2022). A CFD model based on the numerical solution of the Reynolds-averaged Navier–Stokes equations was built using Gmsh (Geuzaine & Remacle 2009), and the OpenFOAM library package (Open Field Operation and Manipulation; Greenshields 2015). The latter provides the freedom to create or modify a specific solver or resolution code, along with pre- and postprocessing tools. In this case, a paraView post-processor was used, enabling the visualization and analysis of data. The simulations were carried out under steady-state conditions, considering a constant Q, and the accuracy of the simulation results was ensured by monitoring the residuals and convergence criteria during the simulations. The Q value was then extracted from the simulations by analyzing the flow field within the flow channel.

Processing time was approximately 10 h for each simulated Q with the purpose of reconstructing the RC. The models aimed at simulating the hydraulic jump had a higher mesh resolution, and the calculation took approximately 2 days.

2.2.3.1. Geometry and meshing model description. The geometry to be solved was considered as a section of the raw water channel, the inlet zone, and the Pf up to the point just before entering the flocculators. The geometry dimensions (width, depth, and channel slope) were obtained from digitized plans and a survey conducted with a Trimble 5,600 total station (Xpert Survey Equipment Ltd), then processed digitally. Based on this fieldwork, plans were prepared according to the actual conditions, which were used to define the geometry and generate the finite volume mesh in Gmsh (Geuzaine & Remacle 2009), and with the snappyHexMesh application of OpenFOAM. The domain was discretized with variable-sized hexahedra (Figure 2), prioritizing higher resolution near the walls and in the water–air interface area.

In this work, a mesh convergence analysis was carried out to determine how the results are modified depending on the cell size used. In particular, the value of the grid convergence index (GCI, Roache 1994) is reported to evaluate the error due to the grid discretization. Three cell sizes were used to discretize the hydraulic jump zone downstream of the Pf: 5, 2.5, and 1.25 cm. In total, each mesh has 279,451, 522,180, and 3,621,625 cells, respectively. The resolution near the walls was increasing to ensure the validity of the wall laws used.

Simulations of a Pf with a similar cell size (3.8 cm) have achieved a deviation of less than 5% when comparing the numerical model and physical model results (Savage *et al.* 2014).

2.2.3.2. Numerical scheme and turbulence model. The interFoam code was employed, designed for a finite volume mesh and two incompressible, isothermal, and immiscible fluids, using a phase-fraction-based interface-capturing approach. The 'Pressure Implicit with Splitting of Operators' algorithm (Issa 1986) was applied as the calculation scheme for pressure and velocity, and successfully adapted for the iterative solution of steady-state problems (Versteeg & Malalasekera 2007). The turbulence closure used was a two-equation k–ω shear-stress-transport (SST) model described by Menter & Esch (2001), considering the additional term F3 (Hellsten 1998), set to zero.

2.2.3.3. Initial and boundary conditions. The numerical scheme requires establishing the following initial and boundary conditions for the fundamental variables: pressure (p), mean velocity ($\bar{U}$, in its three components), turbulent kinetic energy (k), specific rate of turbulent kinetic energy dissipation (ω), and turbulent viscosity (v_t). Initial values were set to zero throughout the domain as the initial condition. Table 2 summarizes the boundary conditions for the inlet, outlet sections, and domain walls. In the inlet section, a constant value of the three components of the velocity vector $\bar{U}$ was set to achieve a constant desired Q, constituting a Dirichlet-type boundary condition. The k–ω SST turbulence model requires values at the inlet section for k, ω, and v_t. These values were estimated based on mean flow parameters: mean velocity, inlet cross-sectional area,
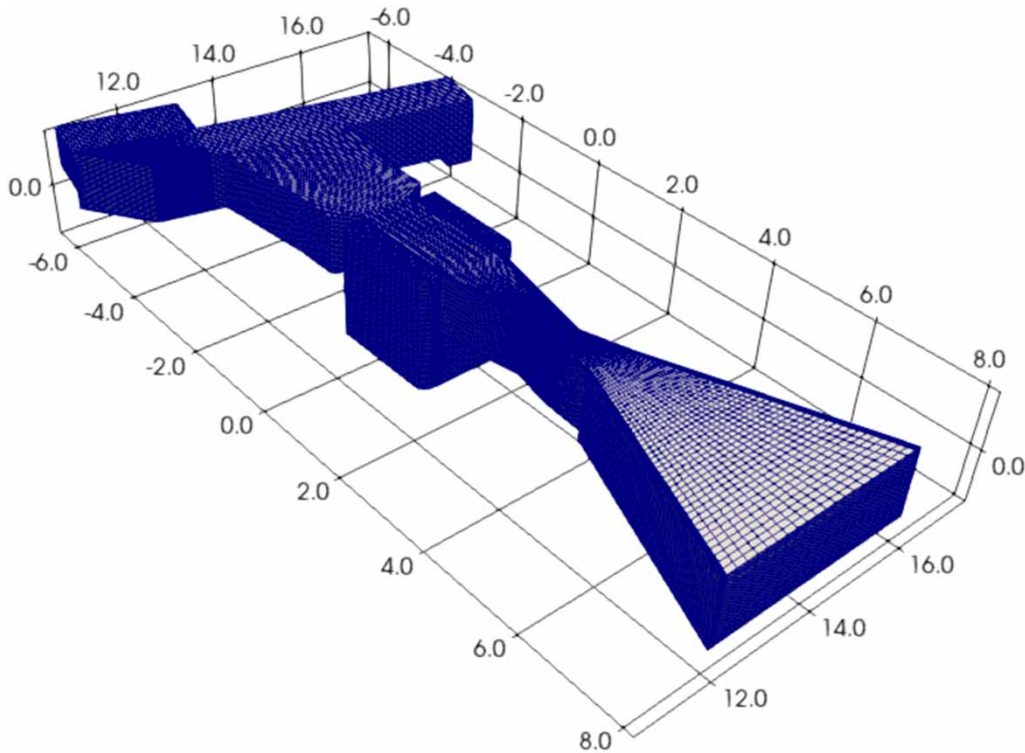
Figure 2 | Finite volume mesh. It includes a section of the raw water channel entrance to the plant, the Pf, and the diverging section where the hydraulic jump occurs.

Table 2 | Boundary conditions of the k–ω SST-RANS numerical model

Surface	$\bar{U}$	p	k, ω, v_t
Inflow	fixedValue	zeroGradient	$k = 1e - 5 \ \mathrm{m^2/s^2}$ $\omega = 0.012 \ \mathrm{s^{-1}}$ $v_t = \text{calculated}$
Outflow	zeroGradient	zeroGradient	zeroGradient
Walls	fixedValue $\bar{U} = (0\ 0\ 0)$	zeroGradient	kqRWallFunction omegaWallFunction nutWallFunction

Names according to the OpenFOAM library.

and turbulence intensity. The CFD-online turbulence property calculator (https://www.cfd-online.com/Tools/turbulence.php) was utilized, and the model then calculated the value of v_t using the provided values for the velocity vectors $\bar{U}$, k, and ω (calculated boundary condition). At the outlet section, a Neumann-type boundary condition was employed for all properties, implying that the gradient in the direction normal to the outlet surface is equal to zero. For the cells of the channel walls and bed, the velocity vector has zero values $\bar{U} = (0, 0, 0)$, while standard wall functions from the OpenFOAM library were used for turbulence properties.

2.2.4. Comparison of rating curves

A comparison was conducted between the SRC and the curve currently employed for the studied Pf, along with those fitted from Q data obtained using SDG, ADV, and CFD. The data analysis method used to compare the different experimental techniques followed the approach of Khosronejad *et al.* (2021). Briefly, a comparative parameter, the percentage difference ($D_{i\text{-SRC}}$) between Q values was calculated as:

$$D_{i-\mathrm{SRC}}(\%) = \frac{Q_i - Q_{\mathrm{SRC}_i}}{Q_i} \times 100 \tag{3}$$

where Q_i is the Q value estimated with every tested curve: CBWTP, SDG, ADV, and CFD, and Q_{SRC} is the Q estimated with the SRC. The values of D_{i-SRC} were contrasted for various values of h to explore differences in Q estimation along the normal operation discharge interval.

2.3. Rapid mixing

The average velocity gradient (G) and residence time (T) in the Pf were calculated (Bratby 2016), considering both standard measures and those obtained from on-site plans. Additionally, G was estimated using the numerical model, which allows for the calculation of turbulent flow parameters, including turbulent kinetic energy (k) and its dissipation rate (ε). The k–ω SST model solves an equation for the specific dissipation rate of turbulent kinetic energy (ω). Therefore, to calculate the dissipation rate ε, the standard coefficient C_μ (equal to 0.09) is used for the turbulence model and $\varepsilon = C_\mu k\omega$. Using these, along with the fluid viscosity (v), the velocity gradient can be estimated as $G = (\varepsilon/v)^{1/2}$ (Ragessi *et al.* 2019). The G values are the result of integrating this property into the volume of the hydraulic jump, for this purpose, the ParaView integrateVariables filter was used. These results were compared with those obtained from on-site plans and standard measures, calculating the percentage difference using, but substituting Q values with G values in Equation (3).

To determine how the results are modified depending on the cell size, a mesh convergence analysis was carried out simulating a 400 L/s Q through the Pf. The representative cell length for each mesh (h_{cell}) and the refinement ratio (r) are indicate: $h_{cell} = 1/N \sum V_p^{1/3}$, where N is the number of cells and V_p is the volume of each cell, and r is calculated as the ratio between the cells size of meshes 1–2 and 2–3. Based on simulation results for mesh 1, 2, and 3, the order of convergence (P), the GCI (GCI$_{21}$: Equation (4)), and the extrapolated relative error (e_{21}^{ext} Equation (5)) were calculated according to the Richardson extrapolation method (Roache 1994) for h_1, Fr$_1$, and G.

$$\text{GCI}_{21} = \frac{1.25 e_{21}}{r^P - 1} \tag{4}$$

$$e_{21}^{ext} = \left| \frac{\phi_1 - \phi_0}{\phi_0} \right| \tag{5}$$

where ϕ_1 is the flow quantity computed from mesh 1 (in this case, h_1, Fr$_1$, and G) and ϕ_0 is the flow quantity extrapolated solution. The order of convergence (P) is calculated from Equation (6) iteratively.

$$\frac{1}{\ln(r_{21})} \left| \ln\left|\frac{e_{32}}{e_{21}}\right| + \ln\left(\frac{r_{21}^P - s}{r_{32}^P - s}\right) \right| - P = 0 \tag{6}$$

where e_{32} and e_{21} are the relative error between meshes 2–3 and 1–2, respectively, r is the refinement ratio between meshes, and s is the sign of the relative error.

3. RESULTS

3.1. Verification of the rating curves

3.1.1. Flow rate estimation by SDG

The instrument was configured to acquire a time series at a frequency of 1 Hz for EC measurement. This setup, coupled with the high resolution of this variable measurement, enhances the signal-to-noise ratio and reduces uncertainty in the estimation of Q (Figure 3).

The Q estimations made with this methodology were performed at the average, minimum, and maximum values of h within the usual operating range of the Pf. The determined Q values are shown in Table 3.

3.1.2. Flow rate estimation by ADV

Eleven Q estimations were made within a range of h from 0.11 to 0.57 m. Velocity measurements were made in the converging section of the Pf, where it is connected with the stilling well (Figure 1). The h, Q pairs recorded using ADV are shown in Table 4.
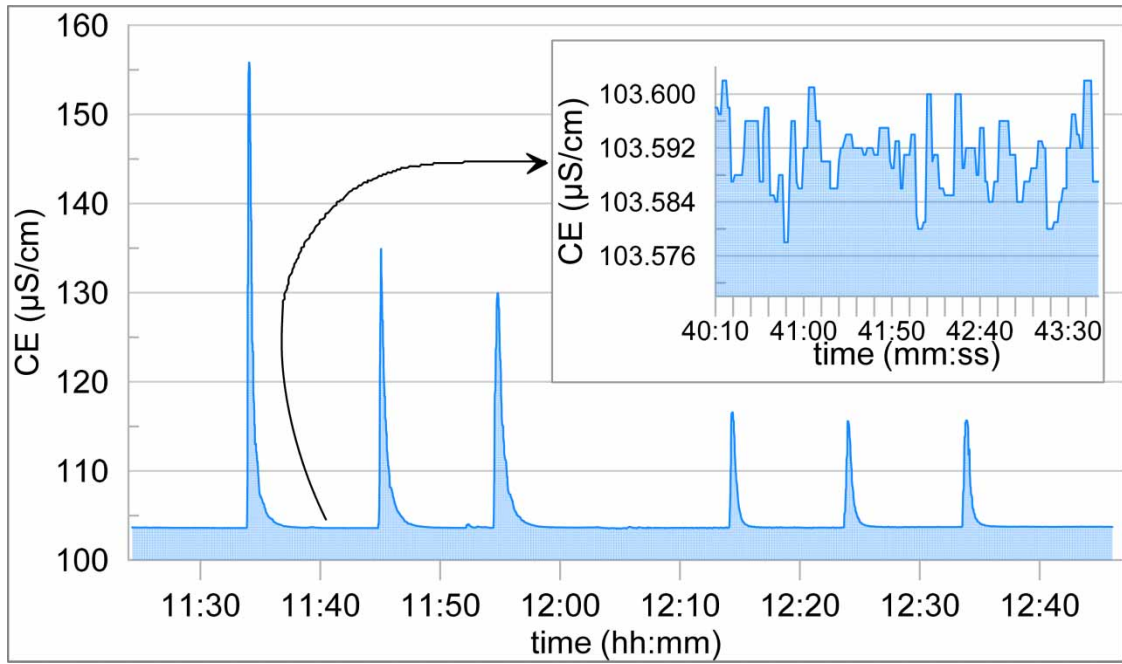
Figure 3 | Record of the temporal variation of EC in one of the probes during tracer solution injection tests for estimating Q using SDG. The main figure shows peaks corresponding to six consecutive injections. The inset displays a seemingly homogeneous section of the time series on a smaller time scale, where the high resolution of the equipment can be observed.

Table 3 | Flow rate estimations using the SDG in the Pf at the Cuesta Blanca Plant

Pf stage height (m)	0.26			0.47					0.55		
Flow rate (L/s)	168	196	192	431	460	421	434	423	573	548	527
Uncertainty (%)	3.4	3.6	3.6	6.0	6.8	3.7	3.8	3.4	3.5	3.7	3.6

Table 4 | Flow rate estimations conducted with ADV at the head measurement section of the Pf

Pf stage height (m)	Flow rate (L/s)	Area (m²)	U (m/s)	Uncertainty (%)	(L/s)	Fr	Date	Time
0.11	21	0.12	0.18	12.3	3	0.17	02 November 2021	10:22
0.15	85	0.19	0.45	7.3	6	0.37	02 November 2021	7:12
0.36	361	0.42	0.86	2.0	7	0.46	20 April 2021	9:20
0.42	380	0.43	0.88	3.2	12	0.43	22 August 2022	12:58
0.47	404	0.44	0.92	3.4	14	0.43	14 December 2021	6:59
0.47	466	0.48	0.97	6.6	31	0.45	24 November 2022	10:20
0.48	438	0.47	0.94	3.2	14	0.43	18 March 2021	11:30
0.48	461	0.48	0.96	1.4	6	0.44	25 October 2021	11:10
0.48	425	0.46	0.93	3.2	14	0.43	10 November 2022	11:30
0.48	394	0.43	0.92	3.1	12	0.42	14 November 2022	11:19
0.49	438	0.47	0.94	3.0	13	0.43	28 January 2022	9:31
0.53	500	0.50	1.00	2.3	12	0.44	16 June 2021	12:00
0.53	527	0.51	1.03	2.5	13	0.45	26 November 2021	10:33
0.57	562	0.53	1.06	2.1	12	0.45	28 January 2022	10:21

U, velocity in the section; uncertainty calculated according to Cohn *et al.* (2013); Fr, Froude number.

3.1.3. Flow rate estimation by CFD

The model projected the evolution of three-dimensional turbulent flow within the measuring section caused by the 90° bend in the inflow channel (see Figure 4). This curvature induced an eddy occupying half of the channel width. Furthermore, turbulence emerged due to subsidence of the channel floor in the chamber where the secondary water intake enters, upstream of the converging section. The model anticipated a nonuniform velocity distribution in the throat section, which persisted along the channel. This phenomenon corresponded with the observations from the ADV Q estimations.
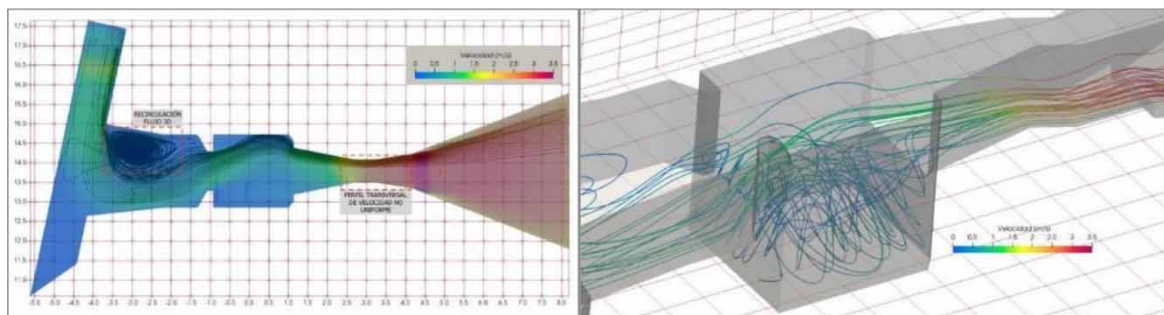

Figure 4 | Simulation of the velocity field and particle trajectory through the Pf.

3.1.4. Comparison of rating curves

Four RCs were compared with the SRC for a Pf with a 0.61 m throat width, corrected using the coefficient from Heiner *et al.* (2011): (i) the curve currently used in the studied Pf; (ii) the curve obtained from Q estimates by SDG; (iii) the curve obtained from Q estimates by ADV; and the curve obtained from the CFD model (Table 5; Figure 5).

Table 5 | Flow rate (Q) estimations in the Pf using five rating curves (RCs)

h (m)	$Q_{1\text{-std}}$ (L/s)	$Q_{2\text{-CBWTP}}$	$Q_{3\text{-SDG}}$	$Q_{4\text{-ADV}}$	$Q_{5\text{-CFD}}$	$D_{\text{CBWTP-SRC}}$ (%)	$D_{\text{SDG -SRC}}$	$D_{\text{ADV-SRC}}$	$D_{\text{CFD-SRC}}$
0.25	169	185	173	139	167	8.7	2.5	−21.1	−1.2
0.30	224	229	225	193	222	2.3	0.8	−16.1	−0.7
0.35	284	275	282	254	283	−3.4	−0.7	−12.0	−0.2
0.40	349	321	342	322	350	−8.7	−2.0	−8.6	0.1
0.45	419	369	407	397	421	−13.5	−3.1	−5.7	0.4
0.50	494	418	474	479	497	−18.1	−4.2	−3.1	0.7
0.55	572	468	544	567	578	−22.3	−5.1	−0.8	1.0
0.60	655	518	618	662	663	−26.3	−6.0	1.2	1.2
Average	–	–	–	–	–	−10.2	−2.2	−8.3	0.2

$Q_{1\text{-std}}$, corrected SRC (Heiner *et al.* 2011); $Q_{2\text{-CBWTP}}$, RC currently used in the treatment plant; $Q_{3\text{-SDG}}$, RC fitted by SDG; $Q_{4\text{-ADV}}$, RC fitted by ADV gauging; $Q_{5\text{-CFD}}$, RC fitted by numerical modeling. The relative differences between standard and experimental rating curves ($D_{i\text{-SRC}}$) for the typical operating range of h and average relative differences are also shown.

The comparison shows that the RC currently used in the studied Pf deviates from the standard curve, underestimating Q for $h > 0.35$ m, i.e. for most of the operating time. Regarding the estimations made with instrumental measurements (SDG and ADV), a good fit was observed for both curves staying within the $\pm 10\%$ interval for Q values. The RC showing the highest correlation coefficient with the tested h values and an average relative difference to the SRC of less than 5% was the one fitted using SDG. Finally, the curve obtained from the numerical model had an almost identical fit to the standard curve.
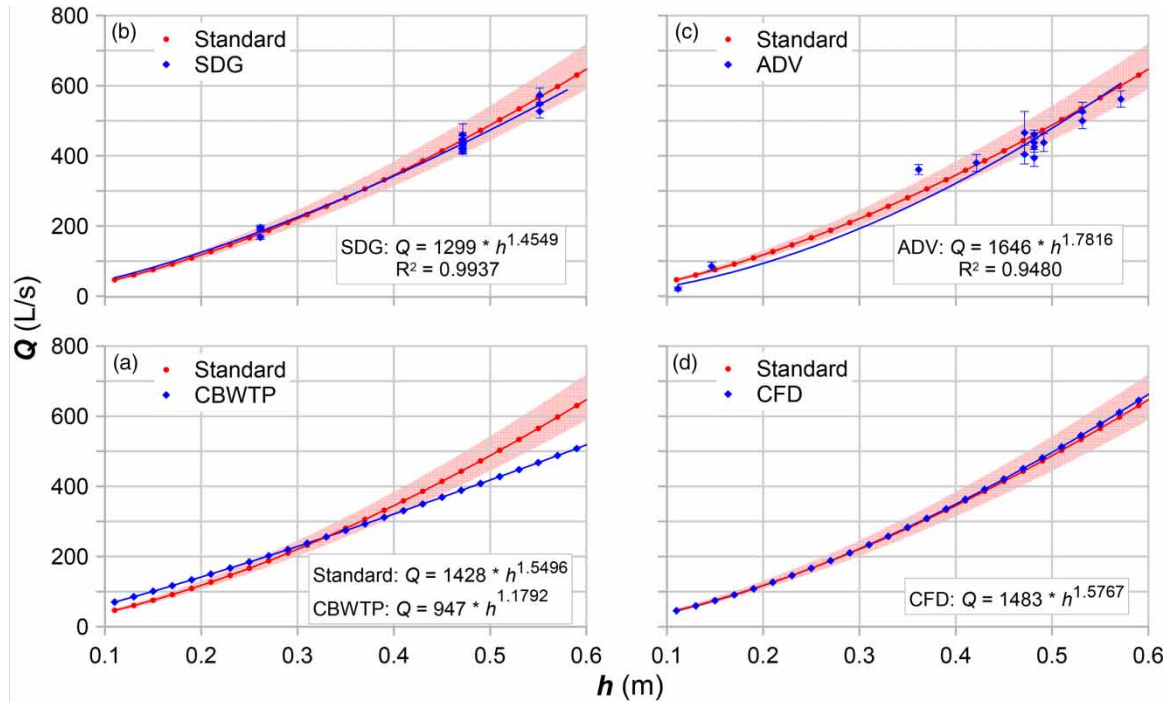
Figure 5 | RCs for the Pf at the intake of the CBWTP and their fitting to respective power functions. The corrected SRC (Heiner *et al.* 2011) for a 0.61 m wide throat Pf (standard) is shown, with the $\pm 10\%$ interval shaded in red. (a) RC currently used in the CBWTP; (b) RC fitted to SDG data, including error bars; (c) RC fitted to ADV tests, also including error bars; and (d) RC obtained from numerical modeling (CFD).

3.2. Rapid mixing

The hydraulic jump in a standard Pf and the studied flume were analyzed through calculations and comparisons of hydraulic residence time (T), Froude number (Fr), and velocity gradient (G) at $Q = 400$ L/s (Table 6; Supplementary Table S1).

Table 6 | Values of rapid mixing parameters in a standard Pf and in the studied device (as-built device) at $Q = 400$ L/s

	Standard device	As-built device	Standard to as-built ratio
Residence time	0.97 s	1.00 s	97%
Froude number	2.20	2.25	97%
Velocity gradient	910 s^{-1}	936 s^{-1}	97%

Standard to as-built ratios are shown.

Velocity gradient values in a grid spanning the volume between the convergent section of the flume and the flow splitter device leading to the flocculators were also obtained from the CFD model. The simulation results for three different meshes are presented in Table 7. Water height (h_1) and Fr$_1$ at the entrance of the hydraulic jump, and G integrated into the volume of the jump.

Table 7 | Simulations results for meshes 1, 2, and 3

Mesh	h_{cell} (m)	r	h_1 (m)	Fr	G (s^{-1})
1	5.73×10^{-7}	6.94	0.180	1.93	1023
2	3.97×10^{-6}	1.87	0.182	1.90	970
3	7.43×10^{-6}	–	0.189	1.85	849

h_1, water height; Fr$_1$, Froude number at the entrance of the hydraulic jump; G, velocity gradient values integrated into the volume of the jump.

The GCI$_{21}$ values for mesh 1 (ϕ_1) are less than 1% from extrapolated solution ϕ_0 (e_{21}^{ext}) h_1, Fr, and G (Table 8), and this indicates that the solutions are well within the asymptotic range of convergence. Also, the extrapolated relative error is less than 1%. Based on this study, we could say that velocity gradient values in the hydraulic jump for 400 L/s Q is estimated to be 1,023 s^{-1} with an error band of 0.8%.

Table 8 | Mesh convergence analysis parameters computed from mesh 1

	P	GCI$_{21}$ (%)	e_{21}^{ext} (%)
G	1.37	0.80	0.63
Fr$_1$	1.57	0.11	0.08
h_1	2.37	0.01	0.01

(ϕ_1), flow quantity; P, order of convergence; GCI$_{21}$, GCI; e_{21}^{ext}, extrapolated relative error.

Finally, using a discretization equal to mesh 1, a flow rate of $Q = 400$ L/s was simulated. Fr$_1$ was estimated and G values were integrated in the hydraulic jump to compare with the values of Table 6. The results show that the G values were highest at the hydraulic jump and decreased in the flow direction (Figure 6). The G values ranged from 500 to 3,000 s^{-1}, with the predominant range in the jump being 1,200–1,300 s^{-1}.
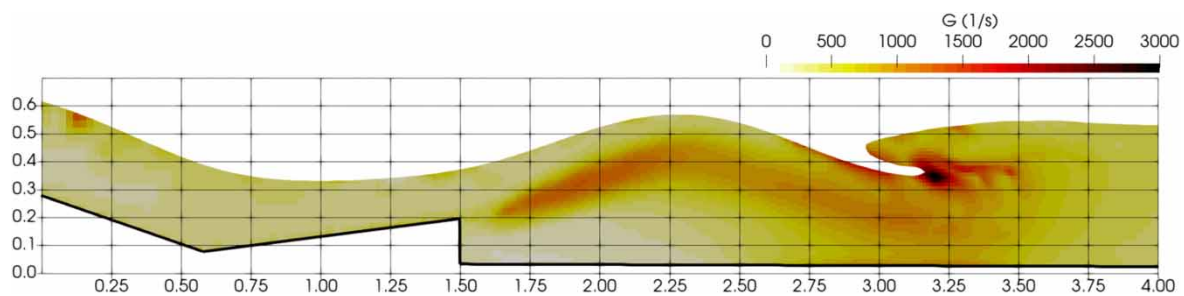

Figure 6 | Longitudinal section of the throat and divergent section of the studied Pf (axis labels in meters. x-axis starting at the convergent section and y-axis at the floor of the outflow channel). Shading represents the velocity gradient (G) along the section, as estimated by CFD modeling.

4. DISCUSSION

4.1. Evaluating the performance of different flow rate estimation techniques under similar flow regime conditions

The comparison of the tested curves against the SRC showed average differences of 0.2, -2.2, -8.3, and -10.2% for those fitted to CFD, SDG, ADV data, and the RC currently in use, respectively (Table 5). These results showed that, with the exception of the RC currently in use, most experimental points in the fitted RCs fall within the $\pm 10\%$ range from the SRC. The statistical similarity between the estimations and models supports their reliability for estimating Q values from h measurements.

The close matching of the CFD RC with the SRC suggests that the used numerical model adequately reproduces the functioning of the device. These findings agree with Heiner *et al.* (2011), Savage *et al.* (2014), Heyrani *et al.* (2021), and Khosronejad *et al.* (2021), who also used RANS models coupled with experimental measures to reproduce flow through Pf. These authors found similar divergences between SRC and modeled RCs and highlighted the usefulness of these tools in analyzing flow patterns in these types of hydraulic structures.

Flow rate estimations using SDG also showed a close match to SRC, with differences ranging from 2 to -6% at low and high Q values (Table 5), demonstrating its utility for verifying Pf operation and RC fitting. This methodology is typically employed in complex geometry channels such as mountain streams (Aubry-Wake *et al.* 2022), where the highly irregular transverse profile renders the velocity–area method unsuitable. Although SDG is commonly used in these hydraulic configurations, studies reporting its utility for evaluating Pf assessment in the

waterworks industry are still lacking. The results reported here suggest that this method could serve as a relatively simple and economical alternative for small water treatment facilities compared with other methods that typically require specialized computational programming skills or expensive apparatus, such as CFD or ADV.

In the present study, Q estimations made with ADV were slightly more scattered when compared with the SDG data. The uncertainty can be attributed to the fact that the turbulent flow through the gauging section (i.e. three-dimensional flow) does not completely satisfy the velocity potential profile assumption at 1/6 (González *et al.* 1996). In addition, since the probe is mounted on a wading rod, it was complicated to keep it stationary due to the high flow velocity. Nevertheless, the RC had a relatively good fit (Figure 5), and in general, higher percentage uncertainties were observed at lower Q values (Table 4). This situation may be related to the computation method of this magnitude, which considers, for each of the verticals, the standard deviation of the mean velocity, which is often higher in a section with a smaller depth due to the effect of turbulence in the water column (Cohn *et al.* 2013). For the rest of the estimations, the uncertainty is less than 5%, which is acceptable for estimations with this instrument (Water Survey of Canada 2015).

4.2. Assessing the impact of using an SRC on Q readings in a nonstandard device

The construction of a Pf, like any measurement device, requires specific conditions to ensure its proper functioning. Among these conditions, it has been established that the approach flow must be calm and orderly to minimize turbulent flow instabilities and ensure a uniform velocity distribution (ISO 1992; USBR 2001). To meet this requirement, a length of 10–20 times the throat width upstream of the device should be free of obstructions or abrupt changes in the channel section (ASTM 2001). In the initial analysis of the studied flume, hydraulic singularities upstream of the device were identified that could potentially generate differences between the measured and calculated Q using the SRC. However, despite observing turbulent flow and a nonuniform flow velocity profile in the gauge section, the similarity between the RCs obtained through different tested methods and the SRC suggests that this does not significantly affect the h–Q relationship in the examined flume. Khosronejad *et al.* (2021) reached a similar conclusion in a study focused on the influence of turbulence on water level fluctuations in a flume with head measurement in the center of the channel. In the present case study, even less influence is expected since the height measurement is made in a stilling well, where instantaneous level fluctuations are practically imperceptible.

When examining the structure of the flume itself, the installation and construction patterns of the primary system stand out. These patterns establish that discrepancies between standard dimensions and construction dimensions should be less than 2% according to ASTM (2001) or 0.2% according to ISO (1992). In the studied Pf, average discrepancies of 1% were observed between standard and construction dimensions. However, two exceptions arose: first, the height difference between the crests of the convergent and divergent sections, which recorded 9.3 cm in the studied flume in contrast to the standard of 7.6 cm; second, the absence of properly proportioned guide walls at the entrance to the convergent section. Regarding the first discrepancy, while the free discharge condition is met, differences are likely not to substantially affect Q in the gauging section. An example of this is the Montana flume, a type of flume built without a divergent section and widely used in systems with sufficient hydraulic heads (USBR 2001). Still, in the analyzed flume, it must be ensured that the hydraulic jump is located downstream of the mid-portion of the divergent section to maintain free discharge. If this condition is not met, the secondary system should be adjusted to measure the head in the throat and the divergent section and calculate the corresponding correction coefficient (ENOHSa 2001). The second discrepancy with a standard flume was related to the arrangement of the guide walls that connect the channel and the convergent section. In the studied device, these walls are located perpendicular to the flow average direction, generating standing waves at the entrance to the flume and may affect the accuracy of the Q estimation (Savage *et al.* 2014). Experimental studies have shown that this disturbance can be reduced by modifying the guide walls, creating a convexity with a radius of 0.51 m (Xu *et al.* 2022). If modification of the structure is not possible, Q correction coefficients can be used, as done in this study following the recommendations of Heiner *et al.* (2011).

When considering the particularities of the secondary system, it is important to note that its accuracy is influenced by the uncertainty associated with head measurement (USEPA 2017). Comparing results obtained from physical and numerical models, Savage *et al.* (2014) noted that measurements of h taken in the center of the convergent section or on a scale located on the wall produce errors in Q estimation close to 5%; in contrast with h values measured in a stilling well that produce errors close to 2% in Q estimation. However, a problem influencing Q estimation was the discrepancy between the reference level of the stilling well and the bottom of the flume

in the gauging section, as observed in the flume under examination. In this study, by using the SRC adjusted according to the recommendations of Heiner *et al.* (2011), this discrepancy results in an underestimation of Q by approximately 46 L/s, representing almost 9% of the maximum treatment discharge.

4.3. Using numerical and modeling calculation methods to determine the degree of similarity in estimates of G downstream of the hydraulic jump

Rapid or flash mixing is recognized as the most important operation in water treatment facilities as it directly impacts the efficiency of flocculation and sedimentation downstream (Bratby 2016). While various methods can achieve rapid mixing, hydraulic jumps offer an alternative approach where abrupt transitions in the flow regime can generate high shear forces, promoting efficient mixing. To optimize the design and performance of hydraulic jumps for rapid mixing, engineers use the Froude number (Fr), a dimensionless parameter, to characterize the flow regime. Arboleda Valencia (2000) suggests that for the effective application of coagulants in a hydraulic jump, Fr should remain within the ranges of 1.7–2.5 or 4.5–9.0, avoiding values between 2.5 and 4.5 as this can lead to an unstable jump. Similarly, effective mixing depends on two key parameters: velocity gradient (G) and retention time (T). For a Pf with a throat of 0.61 m through which a Q between 400 and 600 L/s passes, G values should be close to 900 s^{-1} (ENOHSa 2001) and T values of less than 5 s (Bratby 2016). Also, in an experiment investigating the coagulation of synthetic wastewater in a hydraulic jump, Al-Husseini *et al.* (2019) found no improvement in performance for G values exceeding 800 s^{-1}. This suggests that for similar applications, G values around 900 s^{-1}, as mentioned earlier, might be sufficient. These estimates are close to the results obtained in this study through calculations and numerical modeling (Tables 6 and 7).

5. CONCLUSIONS

Ensuring the correct functioning of Q estimation devices is fundamental to guaranteeing the efficient operation of the water treatment plant. Improper construction or inaccurate placement of complementary instrumentation like measurement scales can significantly affect the recorded values. Although standardized and validated designs for Q estimation can be found in the manuals, the findings from this study show the importance of contrasting the Q values with independent techniques. The evaluation of the tested Q estimation techniques revealed that CFD, SDG, and ADV methods showed promising accuracy when compared with the SRC. These techniques demonstrated that, except for the RC currently in use in the studied Pf, the experimental points in the fitted RCs mostly fell within the $\pm 10\%$ range from the SRC, indicating reliable performance in estimating Q values from h measurements. The alignment of CFD with the SRC suggests the numerical model's effectiveness in replicating device functionality. These findings are consistent with previous studies and emphasize the potential of using these estimation methods for Q calibration in such gauging devices.

The assessment of the impact of using an SRC on Q readings in a nonstandard device highlighted the importance of proper installation and construction to ensure accurate estimations. Despite upstream hydraulic singularities and deviations from standard construction dimensions, the similarity between the RCs obtained through different methods and the SRC indicates the minimal impact on the h–Q relationship in the analyzed device, likely due to the h measurements being made in a stilling well.

Numerical modeling and calculation methods proved effective in determining the degree of similarity in estimates of G downstream of the hydraulic jump. This study demonstrated that for a Pf with a 0.61 m throat and Q between 400 and 600 L/s, G values close to 900 s^{-1} and T values under 5 s are achievable, validating the use of numerical and modeling methods for analyzing and verifying Pf rapid mixing capabilities.

Future research should focus on further investigating the use of SDG to estimate G with recently developed instruments like the one used in this study. This could provide new tools for assessing mixing characteristics in installations utilizing hydraulic jumps as rapid mixing devices, offering a more affordable and user-friendly option for practitioners compared with traditional methods. The findings from this study suggest potential applications in small water treatment facilities, offering a cost-effective and accurate alternative to traditional methods. Expanding the use of these techniques in diverse hydraulic structures can significantly improve water management practices and operational efficiency.

DATA AVAILABILITY STATEMENT

All relevant data are included in the paper or its Supplementary Information.

CONFLICT OF INTEREST

The authors declare there is no conflict.

REFERENCES

Al-Husseini, T. R., Ghawi, A. H. & Ali, A. H. 2019 Performance of hydraulic jump rapid mixing for enhancement of turbidity removal from synthetic wastewater: A comparative study. *Journal of Water Process Engineering* **30**, 100590.

Arboleda Valencia, 2000 *Teoría y Práctica de la Purificación del Agua (Theory and Practice in Water Purification)*. Santa Fe de Bogota, DC: McGraw-Hill.

ASTM 2001 Standard Test Method for Open Channel Flow Measurement of Water with the Parshall Flume. American Society for Testing and Materials, ASTM D1941-01.

Aubry-Wake, C., Pradhananga, D. & Pomeroy, J. W. 2022 Hydrological process controls on streamflow variability in a glacierized headwater basin. *Hydrological Processes* **36**(10), e14731.

Boiten, W. 2003 *Hydrometry: IHE Delft Lecture Note Series*. CRC Press.

Bratby, J. 2016 *Coagulation and Flocculation in Water and Wastewater Treatment*. IWA Publishing.

Cohn, T. A., Kiang, J. E. & Mason Jr, R. R. 2013 Estimating discharge measurement uncertainty using the interpolated variance estimator. *Journal of Hydraulic Engineering* **139**(5), 502–510.

Davis, M. L. 2019 *Water and Wastewater Engineering: Design Principles and Practice*. McGraw-Hill Education.

ENOHSa (Ente Nacional de Obras Hídricas de Saneamiento) 2001 *Guías Para la Presentación de Proyectos de Agua Potable. Ministerio de Obras Públicas (Guidelines for the Presentation of Drinking Water Projects)*. Presidencia de la Nación, Buenos Aires.

Geuzaine, C. & Remacle, J. F. 2009 Gmsh: A 3-D element mesh generator with built-in pre- and post-processing facilities. *International Journal for Numerical Methods in Engineering* **79**(11), 461–477.

González, J. A., Melching, C. S. & Oberg, K. A. 1996 Analysis of open-channel velocity measurements collected with an acoustic Doppler current profiler. In *1st International Conference on New/Emerging Concepts for Rivers*. IWR Association, Chicago, USA

Greenshields, C. J. 2015 OpenFOAM user guide. OpenFOAM Foundation Ltd, Version 3(1), 47.

Heiner, B. J., Barfuss, S. L. & Johnson, M. C. 2011 Flow rate sensitivity due to Parshall flume staff gauge location and entrance wing wall configuration. *Journal of Irrigation and Drainage Engineering* **137**(2), 94–101.

Hellsten, A. 1998 Some improvements in Menter's k-omega SST turbulence model. In *29th AIAA Fluid Dynamics Conference, AIAA-98-2554*.

Hendricks, D. 2011 *Fundamentals of Water Treatment Unit Processes: Physical, Chemical, and Biological*. CRC Press.

Heyrani, M., Mohammadian, A. & Nistor, I. 2021 Numerical simulation of flow in Parshall flume using selected nonlinear turbulence models. *Hydrology* **8**(4), 151.

Heyrani, M., Mohammadian, A., Nistor, I. & Dursun, O. F. 2022 Application of numerical and experimental modeling to improve the efficiency of Parshall flumes: A review of the state-of-the-art. *Hydrology* **9**(2), 26.

ISO (International Standards Organization) 1992 *Measurement of Liquid Flow in, Open Channels – Parshall and SANIIRI Flumes, ISO 9826*. International Standardization Organization, Geneva.

ISO (International Standards Organization) 2007 *Hydrometry. Measurement of Liquid Flow in Open Channels Using Current-Meters or Floats. ISO/TS 748:2007*. ISO, Geneva.

Issa, R. I. 1986 Solution of the implicitly discretised fluid flow equations by operator-splitting. *Journal of Computational Physics* **62**(1), 40–65.

Khosronejad, A., Herb, W., Sotiropoulos, F., Kang, S. & Yang, X. 2021 Assessment of Parshall flumes for discharge measurement of open-channel flows: A comparative numerical and field case study. *Measurement* **167**, 108292.

Masschelein, W. J. 1992 *Unit Processes in Drinking Water Treatment*. CRC Press, New York.

McCabe, W. L., Smith, J. C. & Harriot, P. 2005 *Unit Operations of Chemical Engineering*. McGraw-Hill, New York.

Menter, F. R. & Esch, T. 2001 Elements of industrial heat transfer predictions. In *16th Brazilian Congress of Mechanical Engineering (COBEM)*, Uberlandia.

Moore, R. D. 2005 Slug injection using salt in solution. *Streamline Watershed Management Bulletin* **8**(2), 1–6.

Pant, H. J., Goswami, S., Biswal, J., Samantray, J. S. & Sharma, V. K. 2016 Discharge rate measurements in a canal using radiotracer methods. *Applied Radiation and Isotopes* **112**, 89–97.

Ragessi, I. M., García, C. M., Márquez Damián, S., Pozzi Piacenza, C. & Cantero, M. I. 2019 Detailed experimental and numerical characterization of turbulent flow in components of a water treatment plant. *Water Science and Technology* **80**(11), 2117–2130.

Richardson, M., Sentlinger, G., Moore, R. D. & Zimmermann, A. 2017 Quantifying the relation between electrical conductivity and salt concentration for dilution gauging via dry salt injection. *Confluence: Journal of Watershed Science and Management* **1**(2).

Roache, P. J. 1994 Perspective: a method for uniform reporting of grid refinement studies. *ASME Journal of Fluids Engineering* **116**(3), 405–413. https://doi.org/10.1115/1.2910291.

Saran, D., Tiwari, N. K., 2022 Generation of a versatile discharge formula for multiple Parshall flumes using a regression technique. In: *Advances in Mechanical and Materials Technology. EMSME 2020. Lecture Notes in Mechanical Engineering* (Govindan, K., Kumar, H. & Yadav, S., eds), Singapore, Springer. https://doi.org/10.1007/978-981-16-2794-1_104.

Savage, B. M., Heiner, B. & Barfuss, S. L. 2014 Parshall flume discharge correction coefficients through modelling. *Proceedings of the Institution of Civil Engineers-Water Management* **167**(5), 279–287.

Sentlinger, G., Fraser, J. O. H. N. & Baddock, E. V. A. N. 2019 Salt dilution flow measurement: Automation and uncertainty. In *HydroSenSoft, International Symposium and Exhibition on Hydro-Environment Sensors and Software*, Vol. 8, p. 8.

Silva Ribeiro, Á., Sousa, J. A., Simões, C., Martins, L. L., Dias, L., Mendes, R. & & Martins, C. 2021 Parshall flumes flow rate uncertainty including contributions of the model parameters and correlation effects. *Measurement: Sensors* **18**, 100108.

USBR (US Bureau of Reclamation) 2001 *Water Measurement Manual; A Water Resources Technical Publication*. Available from: https://www.usbr.gov/tsc/techreferences/mands/wmm/WMM_3rd_2001.pdf (accessed 13 December 2023).

USEPA (US Environmental Protection Agency) 2017 *NPDES Compliance Inspection Manual*. US Environmental Protection Agency, Office of Water, Office of Water Enforcement and Permits. EPA 305-K-17-001.

USGS (US Geological Survey) 2004 *Policy on the Use of the FlowTracker for Discharge Measurements: Technical Memorandum 2004.04*. USGS, Washington, DC.

Vatankhah, A. R. 2022 General free-flow discharge equation for parshall flumes. *Proceedings of the Institution of Civil Engineers-Water Management* **175**(5), 257–270.

Water Survey of Canada 2015 *Measuring Discharge with FlowTracker Acoustic Doppler Velocimeters – Revision 4, qSOP-NA022-04-2015*. Environment Canada, Ottawa.

Wright, S. J., Tullis, B. P. & Long, T. M. 1994 Recalibration of Parshall flumes at low discharges. *Journal of Irrigation and Drainage Engineering* **120**(2), 348–362.

Xu, H., Li, Z., Wu, W., Liu, T., Hu, Y. & Ma, M. 2022 Hydraulic characteristics of the Parshall flume entrance wingwall: Numerical simulation and test. *Irrigation and Drainage* **71**, 1280–1293.